ISSN 1063-7729, Astronomy Reports, 2010, Vol. 54, No. 3, pp. 254–259. © Pleiades Publishing, Ltd., 2010.
Original Russian Text © A.V. Getling, A.A. Buchnev, 2010, published in Astronomicheskiĭ Zhurnal, 2010, Vol. 87, No. 3, pp. 286–292.

Some Structural Features of the Convective-Velocity Field in the Solar Photosphere

A. V. Getling[1] and A. A. Buchnev[2]

[1] *Institute of Nuclear Physics, Moscow State University, Moscow, 119991 Russia*
[2] *Institute of Computational Mathematics and Mathematical Geophysics, Novosibirsk, 630090 Russia*

Received September 25, 2009; in final form, October 19, 2009

Abstract—An algorithm for measuring horizontal photospheric velocities previously employed to process aerospace images is adapted for problems in solar physics and realized in a computational code. It differs from the standard procedure of local correlation tracking in a special choice of trial areas ("targets"), whose displacements are determined by maximizing the correlation between the original and various shifted positions of the target. Specifically, an area is chosen as a target in a certain neighborhood of each node of a predefined grid if either the contrast or the entropy of the brightness distribution reaches its maximum in this area. The horizontal velocities obtained are then interpolated to the positions of imaginary "corks" using the Delaunay triangulation and affine transformations specified by the deformation of the obtained triangles at the time step considered. The motion of the corks is represented by their trajectories. A superposition of flows on different scales, from mesogranular to supergranular, can clearly be seen. "Large mesogranules" with sizes of order 15 Mm are revealed. In many cases, these are stellate in shape. Areas of strong convergence of the horizontal flows are detected; this convergence is sometimes accompanied by swirling. Evidence is found for the possible coexistence of convection cells with different circulation directions, so-called *l*-type and *g*-type cells.

DOI: 10.1134/S1063772910030078

1. INTRODUCTION

The abundant observational data supplied by space stations and describing solar chromospheric and coronal phenomena have stimulated active interest in these phenomena. As a result, studies of photospheric and subphotospheric flows, which are directly observable (rather than requiring reconstruction from helioseismological data), were somewhat pushed into the background. The active processes in the photospheric and subphotospheric layers are not as violent as in the overlying layers, so that the dynamics there seem, in principle, relatively clear and not requiring detailed analysis.

At the same time, the magnetic fields responsible for the entire complex of active phenomena originate in dense layers of the Sun, where flows play an important role in the formation of these magnetic fields. The structure of these fields is largely an imprint of the flow structure, and must be understood if we are to understand solar-activity processes.

The convective motions in these dense layers are complex and poorly ordered. It may be precisely this fact that has relegated the problem of their morphology to the background. However, as will become clear from the material considered here, if proper techniques are chosen, the structural organization of the flows can become quite pronounced and demonstrate some remarkable properties.

Four well-known types of cells observed on the Sun are usually associated with thermal convection, viz., granules, mesogranules, supergranules, and giant cells. Their principal parameters are listed in the table. The question mark entered for the velocity typical of granules emphasizes that the velocities inside the granules and the velocities of the granules themselves cannot easily be separated in these highly mobile and changeable features. Since the granules are transported by larger-scale flows, they can be used as tracers to investigate the structure of these flows [1–4].

This fact (and, generally, the transport of brightness inhomogeneities by matter flows) underlies the widely known method of *local correlation tracking* (LCT) for measuring the velocities of brightness-field features [5]. To some extent, these velocities correspond to the matter flow velocities and can be used instead of the latter in analyses of the photospheric dynamics (note that no method for directly measuring velocities normal to the line of sight has been developed; obviously, the motion of brightness inhomogeneities is not the same thing as the motion of the matter).

In our opinion, patterns of motion of imaginary "*corks*" represent most informatively the velocity fields obtained using the LCT technique. The corks are initially assumed to be uniformly distributed over the image, and their further motion is determined at any time using the local velocities found.

Time series of maps of the cork distributions indicate that condensations of these particle outline progressively larger cells with time [6]. However, the enlargement of the cells appears to be a continuous process, and such series cannot be used to study the shapes and characteristic sizes of true cells in the velocity field. This can be understood in general terms from the following considerations. As they reach those sections of their trajectories where the vertical velocity component (downflow) dominates, the particles collect there, since they can move only horizontally. The larger the flow scale, the longer this flow persists and the more particles accumulate at downflow sections, outlining the contours of the flow cells. However, before the particles reach these sections, they can be collected by unsteady, intermediate-scale flows. In this case, a cellular pattern can also develop; however, the cells outlined by the cork pattern will be stretched by the larger-scale flows. Therefore, the scale of the visualized cells will continuously grow, and the larger-scale flows will become progressively more pronounced. If this analysis method is used, the velocity-field components for different scales cannot easily be separated.

As we will see, it is much better to map the cork trajectories instead of plotting the instantaneous cork distributions in the horizontal plane.[1] In this case, the short-lived flows will only produce some jittering of the particle that causes their trajectories to meander, whereas, after a sufficiently long time, the endpoints of these trajectories will be gathered, outlining the features most stable over the given time interval.

The LCT method—in both its traditional form and the improved version employed here—will be briefly described in the next section. The technique used by us was originally developed for space hydrometeorology and was applied to determining the velocities of cloud masses and drifting ice [7]; it was later adapted for problems in solar physics. We will track the motion of corks in the velocity field obtained by analyzing a series of granulation images.

[1] Strictly speaking, the plane of the sky is meant here. However, images obtained near the solar-disk center should be used to study horizontal flows; thus, we will make no distinction between the plane of the sky and the horizontal plane on the Sun.

Principal parameters of the velocity-field cells on the Sun

Cell type	Size, Mm	Lifetime	Horizontal velocities in the cell
Granules	0.25–2	8–15 min	1–2 km/s (?)
Mesogranules	5–10	2–10 h	0.4–1 km/s
Supergranules	20–30	$\gtrsim$1 day	$\sim$500 m/s
Giant cells	Hundreds	$\gtrsim$100 days	$\sim$4 m/s

2. TECHNIQUES

The idea of the LCT method is as follows (Fig. 1). An area, A, is chosen in an image of the solar surface. Another image taken shortly after the first image is then considered. Variously shifted positions are inspected in some neighborhood of the initial position of area A. For each of these, the correlation between the brightness distributions over the original area in the first image and over the shifted area in the second image is calculated. In Fig. 1, the brightness pattern inside the original area is shown as a shaded feature outlined with a solid curve. Let us suppose that this correlation is maximum at some shifted position, B, among all the values obtained for various shifts (the brightness pattern in the shifted area is represented by the shaded region outlined with a solid curve, whereas the original shaded region shifted together with the area is outlined with a dashed curve; clearly, the less the shifted pattern differs from the original one, the higher the correlation). In this case, the shift vector (shown as the heavy arrow) of area B with respect to area A divided by the time interval between the times when the two images were taken is regarded as the local velocity vector.

The procedure we employ here differs from the standard LCT procedure in our choice of the trial areas ("targets") used to calculate the correlations. While, in the standard method, the targets are fixed to the nodes of a purposely specified uniform grid, the choice of the targets in our study is a particular problem.

We choose our target to be a square area in the image, such that the brightness in this area is "maximally variable" compared to the neighboring areas. Our search for targets is based on the EUMETSAT technique [7]. The search for targets using this technique employs the size of the square grid cells, $Grid\_Size$; the size of the square area centered at the grid point and used to search for the targets, $Targ\_Search$; the size of the target, $Targ\_Size$; and the minimum distance between target centers, $Targ\_Dist$ (the targets may partially overlap). We

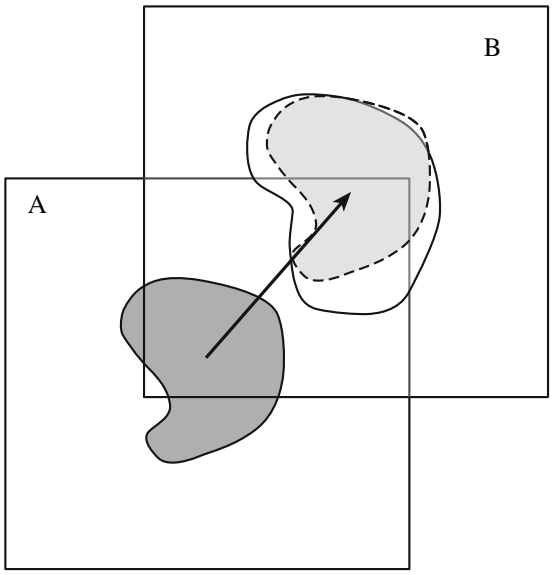

Fig. 1. Illustration of the principle of measuring velocity using the technique of local correlation tracking. See the text for explanation.

regard the position where the control parameter Par, which is either the contrast or the entropy, reaches its maximum as the optimum target position in the search area. To search for targets in an area of size $Targ\_Search$, we use the local brightness averages I calculated for each point in a surrounding neighborhood of 3×3 pixels and the local standard deviations (in the same neighborhood). The contrast is defined as the difference

$$C = I_{\max} - I_{\min}, \tag{1}$$

where $I_{\max}$ and $I_{\min}$ are the maximum and the minimum local brightness in the area. The entropy is

$$E = -\sum_i p_i \log p_i, \tag{2}$$

where p_i is the probability of a pixel of value i; [2] the summation is done over all pixels in the area with different values. This probability is defined as $p_i = S_i/S$, where S is the image area (the number of pixels) and S_i is the number of pixels of value i in the image.

In addition to the above geometrical parameters, we selected targets using also the following characteristics of the image variability in the area covered by the target: Min_St_Dev, the minimum value of the local standard deviation, and Num_Gr_SD, the minimum number of pixels with a standard deviation in excess of Min_St_Dev. The shift is determined for each of K_Targs targets found. The new target position is sought inside the square area of size $Search\_Size$ whose center coincides with the original position of the target. We regard the position where the correlation coefficient $Corr$ reaches its maximum as the new target position. In contrast to the technique of EUMETSAT [7], we allow scaling and rotation transformations of the target in the process of scanning the search region. Among all the new positions found, we can select those satisfying the threshold conditions; more precisely, we specify the minimum admissible correlation coefficient and minimum admissible target shift.

The use of such selection criteria for the targets reduces the probability of considering brightness distributions over areas with weak and smooth brightness variations that are correlated by chance. This ultimately increases the reliability of local-velocity determinations.

To compare the velocity fields for different times, we must obtain the velocity values for the same points; to plot trajectories, the velocities must be determined for the endpoints of the already constructed segments of the trajectories. However, our procedure yields velocities for the points specified by our choice of targets, which are different at different times. For this reason, we obtained the velocities for the needed points by interpolating the horizontal velocities found using our technique to these points. To this end, we constructed a Delaunay triangulation (see, e.g., [8]) on the family of the original target positions and the affine transformations specified by the deformation of the constructed triangles at the time step considered.

Previously, Pötzi [9] plotted cork trajectories using the standard LCT procedure. We used one of the maps of trajectories he obtained based on the same series of granulation images that we process here to test our algorithm. As far as we know, Pötzi did not employ the maps of trajectories to analyze the flow structure.

Here, we plot the trajectories based on the modified LCT algorithm described above to study the morphology of the solar convection.

3. OBSERVATIONAL DATA

We analyzed a series of solar-granulation images obtained on June 5, 1993 by Simon et al. [10] using the Swedish Vacuum Solar Telescope (La Palma, Canary Islands). This series is remarkable in terms of its duration (11 h), continuity (a constant frame cadence of 21.03 s), and quality (rms contrast varying from 6 to 10.6%), taken together, and remains among the best available. The observations were carried out from 08:07 UT to 19:07 UT near the center of the solar disk in a 10-nm spectral band centered at 468 nm.

[2] For brevity, we will write *the pixel value* in place of *the brightness value at the pixel*.

As a rule, the spatial resolution of the images was no worse than 0.5″.

The preprocessing of data included spatial alignment of each image with the preceding image, a destretching procedure required to compensate for atmospheric distortions, and the removal of fast (5-min) intensity variations via subsonic filtering [11]. In addition, after cutting a central area 43.5 × 43.5 Mm in size (480 × 480 pixels 0.125″, or 90.6 km, in size), all the images were normalized to a specified rms contrast chosen to be standard, and the residual large-scale intensity gradient was eliminated from them. We use here a subset of the series covering an interval of duration 8 h 45 min (1500 frames).

4. RESULTS

We present here the results of constructing cork trajectories traversed over intervals of about two hours' duration.

A series of trajectory maps plotted for a sequence of overlapping two-hour intervals is shown in Fig. 2. The motion from the beginning to the end of each trajectory is shown by an increase in the curve brightness. The ends of the trajectories clearly outline the boundaries of cells.

In particular, two cells on a supergranular scale are quite distinct in the upper half of Fig. 2a; another somewhat smaller cell is located below the image center, and a third adjoins it on the left. The boundary of the supergranule located in the lower middle is especially pronounced in Figs. 2b–2d (and a deformation of the supergranule can be noted), and the boundary of the upper-right supergranule in Fig. 2d. The pattern in the other images is more complex, and, although the supergranules can still be outlined, this is more difficult.

Smaller-scale cells can also be distinguished against the supergranular background. For example, the lower supergranule in Fig. 2a is intersected by two (almost perpendicular) lines that are apparently the boundaries of smaller, mesogranular-scale cells. In this image, the shape of these small cells is nearly triangular; they deform at later times. The fact that they are definitely "inscribed" in a supergranule in Fig. 2a suggests that a secondary flow has developed here due to an instability of the supergranule. The idea that we see here a superposition of flows on two different scales is supported by the fact that the left-hand mesogranule (triangular in Fig. 2a and roundish in Fig. 2c) is characterized by an asymmetric trajectory pattern: the trajectories are longer in its left-hand part, where the velocities of the mesogranular flow are added to those of the supergranular flow, than they are in the right-hand side, where these two components cancel each other out.

Thus, the separation of flow scales and the outlines of cells can quite clearly be noted in the trajectory maps. The largest, supergranular, cells are superposed with smaller ones, which can be reliably identified with mesogranules. It is interesting that the shapes of the boundaries of both these types of cells are much closer to polygonal (and, therefore, to the shapes of the cells observable under quiescent laboratory conditions—in particular, in moderately supercritical regimes) than if these boundaries are identified based on the concentrations of corks at a certain time.

The trajectory maps are very convenient for determining the cork velocities (which are presumably the horizontal matter velocities) averaged over the time for the passage of a certain segment of the trajectory. In particular, cork displacements of the order of 6 Mm, typical of the detected mesogranules at the segments of the trajectories obtained from the data for a two-hour interval, yield velocities of the order of 0.8 km/s. This is within the range of mesogranular velocities. However, when making such velocity estimates, we must bear in mind that the trajectory results from a superposition of flows on different scales, and the separation of the velocities related to different sorts of cells is, in general, a special problem.

It can easily be seen from Figs. 2a and 2b that the two upper supergranular cells are superposed with cells that are considerably smaller (about 15 Mm in size), but appreciably exceed the sizes typical of mesogranules. The cell superposed onto the right-hand supergranule is even more pronounced in Fig. 2d. We are not aware of references to such cells in the literature. These cells, which we tentatively call "large mesogranules," can be detected at various times and do not appear to be a rare phenomenon. While the supergranules resemble convex (typically irregular) polygons, the large mesogranules can also exhibit stellate shapes (in particular, this can be seen for the cell superposed onto the upper right supergranule in Figs. 2b and 2d). This may testify that the flows in such cells are farther from a well-established regime than the flows in the supergranules, and are characterized by flows diverging from the center.

It is remarkable that several areas with a strong convergence of horizontal flows can be noted in each image. These are mostly at the nodes of the network formed by the cell boundaries (where the matter descends). This is generally typical of convection in the conditions of the formation of well defined polygonal convection cells with central upflows and peripheral downflows. However, in some cases, there is no clear relationship between such areas and the network. For example, near the left edge of the image in Figs. 2b and 2c, at roughly its mid-height, there is a convergence that does not seem to be associated with a node

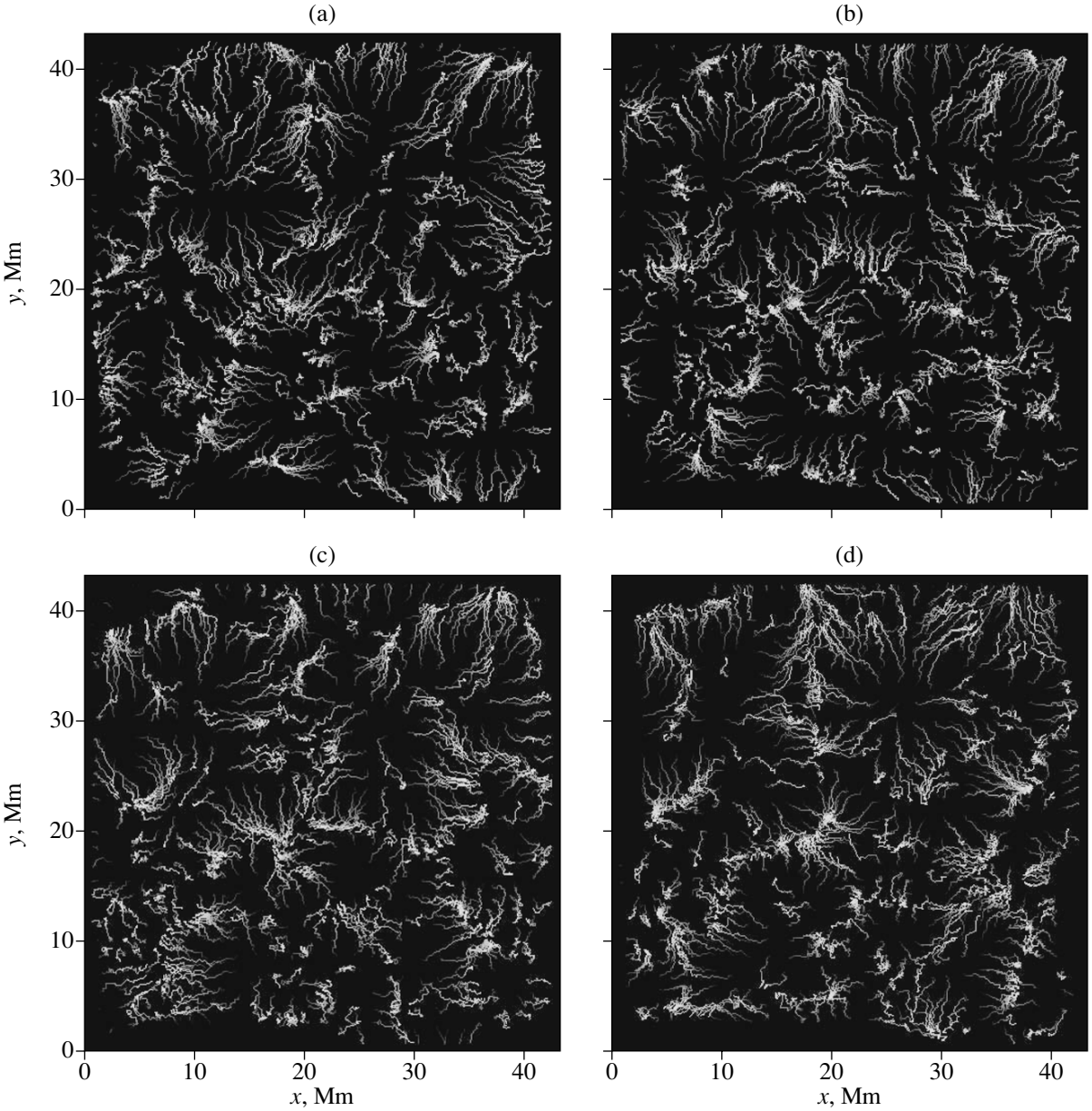

Fig. 2. Trajectories of corks during the time intervals (a) 8:43–10:46 UT, (b) 10:11–12:14 UT, (c) 11:38–13:41 UT, and (d) 13:06–15:09 UT. The motion of a cork from the beginning to the end of the trajectory is shown by an increase in the brightness of the curve.

of the network of cell boundaries. The same is true of the smaller convergence area located somewhat higher.

The presence of such isolated convergence areas raises the question of the character of convective circulation in their vicinity. Obviously, if matter descends rather than ascends at the center of some convection cell, ascends along the edges of the cell, and then moves centripetally, the edges of the cell will not be visible in the trajectory map; on the contrary, a convergence will be visible in the center. Since the convergence areas noted above do not agree with the general network of downflows and are surrounded with a dark background in the figure, it is quite possible that they are located at the centers of mesogranular-scale cells with an opposite (compared to most cells) direction of circulation. We note that precisely such "opposite" circulation is typical of gases under *laboratory* conditions (which differ radically from the solar conditions); therefore, cells with central downflows are called *g*-type (derived from *gas*) cells; in contrast, *l*-type (from *liquid*) cells with central upflows are typical of convection in liquids; see, e.g., [12, Chapter 4], where investigations of the

effects of various factors on the direction of circulation in the cells are reviewed.

Finally, we note another interesting property of the areas of convergence. We can clearly see from Fig. 2c that the flow converging to the hypothetical center of a *g*-type flow swirls in a circular motion. This effect is expected where a concentrated downflow is present (this phenomenon is probably akin to the swirling of water as it is drained from the bath). Vortical flows have already been repeatedly observed in the photosphere; in our case, however, we see a strong convergence of the swirling flow within a very small area, which can hardly be interpreted other than as a manifest of a localized sink.

5. CONCLUSIONS

(1) The construction of cork trajectories based on an improved local-correlation-tracking technique is an effective tool for studying the structure of convective motions in near-photospheric layers. It displays quite clearly a superposition of flows on various scales ranging from mesogranular to supergranular scales.

(2) The shapes of the supergranulation and mesogranulation cells that can be identified in the cork trajectory maps are more similar to ordered convection cells observed under laboratory conditions than cells detected in other ways.

(3) In addition to the supergranulation and mesogranulation cells with characteristic sizes of $\gtrsim$20 and 5–10 Mm, we have detected "large mesogranules" with intermediate sizes of the order of 15 Mm.

(4) In some cases, such cells are stellate in their appearance, which may be an effect of nonstationarity of the convective flows.

(5) Small areas of strong convergence, sometimes with swirling motions, is characteristic of the photospheric flows, which can be revealed by plotting the cork trajectory maps.

(6) It cannot be ruled out that *l*-type and *g*-type cells coexist in the overall convection field.

ACKNOWLEDGMENTS

This work was supported by the Russian Foundation for Basic Research (project no. 07-02-01094).

REFERENCES

1. A. M. Title, T. D. Tarbell, G. W. Simon, and the SOUP Team, Adv. Space Res. **8**, 253 (1986).
2. R. Muller, H. Auffret, T. Roudier, et al., Nature **356**, 322 (1992).
3. R. A. Shine, G. W. Simon, and N. E. Hurlburt, Solar Phys. **193**, 313 (2000).
4. M. Rieutord, T. Roudier, H.-G. Ludwig, Å. Nordlund, and R. Stein, Astron. Astrophys. **377**, L14 (2001).
5. L. J. November, Appl. Opt. **25**, 392 (1986).
6. W. Pötzi, "Dynamics of the Solar Granulation and Mesogranulation," Dissertation (Universität Graz, 2001).
7. *MSG Meteorological Products Extraction Facility. Algorithm Specification Document*, Doc. No. EUM/MSG/SPE/022, Issue 2.6.1 (EUMETSAT, 2004).
8. F. P. Preparata and M. I. Shamos, *Computational Geometry: An Introduction* (Springer, New York, 1985; Mir, Moscow, 1989).
9. W. Pötzi, private commun. (2007).
10. G. W. Simon, P. N. Brandt, L. J. November, et al., in *Solar Surface Magnetism*, Ed. by R. J. Rutten and C. J. Schrijver, Sci. Inst., Adv. Sci. Inst. Ser. C: Mathem. Phys. Sci. **433** (Kluwer, Dordrecht, 1994), p. 261.
11. A. M. Title, T. D. Tarbell, K. P. Topka, et al., Astrophys. J. **336**, 475 (1989).
12. A. V. Getling, *Rayleigh–Bénard Convection: Structures and Dynamics* (World Sci., Singapore, 1998; URSS, Moscow, 1999).

Translated by A. Getling